ACS APPLIED BIO MATERIALS

www.acsabm.org

Forum Article

# Biochar Nanozyme from Silkworm Excrement for Scavenging Vapor-Phase Free Radicals in Cigarette Smoke

Quanyi Liu, Sheng Zhao, Yihong Zhang, Xueying An, Quan Wang, Sirong Li, Anqi Lin, Yan Du,* and Hui Wei*

Cite This: *ACS Appl. Bio Mater.* 2022, 5, 1831−1838

Read Online

ACCESS | Metrics & More | Article Recommendations | Supporting Information

**ABSTRACT:** Serious lung diseases and other health problems caused by tobacco consumption are becoming more and more prominent all over the world. Scavenging the excessive harmful free radicals in cigarette smoke is proven to be an effective method in reducing the above problems. Carbon-based nanozymes have been widely studied due to their ability of scavenging free radicals. Accordingly, the biochar derived from silkworm excrement was reported as a nanozyme with free radical scavenging ability. The biochar nanozyme calcination at 900 °C with better free radical scavenging abilities was loaded into commercial cigarette filters for the following free radical scavenging verification in tobacco smoke. Mouse model results reveal the lung tissue could be improved by the addition of biochar nanozyme. This work not only provides an effective approach to reduce the harm caused by tobacco but also provides potential applications to rationally realize low-cost, ease of production, and a wide variety of biochar sources.

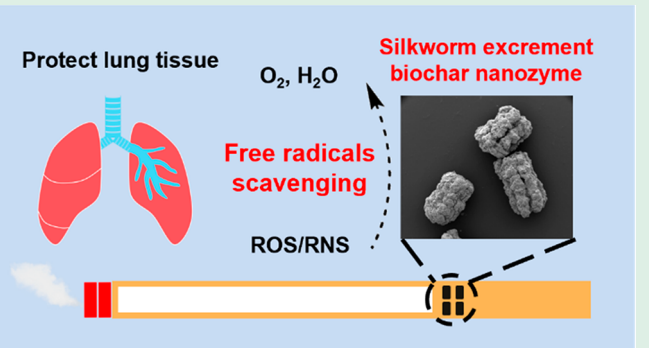


**KEYWORDS:** *biochar nanozyme, silkworm excrement, cigarette smoke, free radicals, acute lung injury*



## 1. INTRODUCTION

Epidemiological and clinical studies have shown that smokers are more likely to suffer from lung cancers, chronic obstructive pulmonary disease (COPD), and other respiratory diseases compared with nonsmokers.[1−3] Yet, smokers still account for a large proportion of the population worldwide.[4] During the process of smoke passing through a cigarette into the lungs, harmful substances, such as free radicals (a class of highly reactive oxidants containing reactive oxygen species (ROS), reactive nitrogen species (RNS), and alkyl radicals, *etc.*), generated and further induced oxidative stress, respiratory system damage, and various diseases.[5−7]

To guard against the oxidant byproducts, antioxidant therapy has been applied in the treatment of COPD and other lung diseases caused by smoking.[8,9] In typical antioxidant therapy, antioxidants (*e.g.*, polyphenols, glutathione, and vitamin C) are administered to prevent oxidative stress by scavenging free radicals and relieving the corresponding harmful effects. However, it is better to scavenge the vapor-phase free radicals in cigarette smoke before they enter and damage the lungs instead of repairing the already damaged lung tissue. We reason that if the vapor-phase free radicals in cigarette smoke could be scavenged by antioxidants when they pass through the cigarette filter, the damage could be effectively avoided from the radicals.

In this regard, we designed a cigarette filter with multiradical scavenging abilities. More importantly, we embed nanozymes, nanomaterials with enzyme-like characteristics, inside the cigarette filter. Nanozymes possess superiority over either antioxidants or natural enzymes.[10−17] For one thing, the commonly used antioxidants in typical antioxidant therapy are consumable and suffer from a fixed stoichiometric antioxidant capacity. For another, the complex composition of radicals requires good negotiation between several antioxidant enzymes, increasing the cost. Also, the heat of burning threatens the structure stability of enzymes and therefore breaks the sustainable process of scavenging radicals. So far, a variety of nanomaterials have been discovered to possess inherent enzymatic catalytic properties, such as noble metals, metal oxides, metal−organic frameworks, and carbon.[18−25] Despite this promise, very few studies have been carried out to load nanozymes in a cigarette filter for scavenging ROS free radicals in cigarette smoke.[26−28] In addition, the RNS scavenging activity of nanozymes has not been paid enough

**Special Issue:** Early Career Forum

**Received:** October 14, 2021
**Accepted:** November 25, 2021
**Published:** December 8, 2021

attention yet. Moreover, huge cigarette consumption means the cost of loaded nanozyme must be economical, and the production process must be facile. Carbon nanozymes have been proven to have excellent antioxidant capacity and are used in lots of antioxidant therapy.[29−38] Among the numerous materials to produce carbon nanozymes, biochar has the advantages of low cost, ease of production, and environmental friendliness.[39] As a natural resource, silkworm excrement (SE) is an abundant byproduct in the silk industry with an annual output of more than 5 million tons. SE could be used to produce biochar by pyrolysis at high temperature.[40,41] Biochar-based nanozymes have not been explored to scavenge free radicals for therapies.

In this work, we reported a calcined SE nanozyme, which simultaneously exhibited superoxide dismutase (SOD)-like activity, catalase-like activity, and nitric oxide free radical ($NO^{\bullet}$) scavenging ability. These synergistic free radical scavenging capabilities combine the advantages as a biochar endowed SE nanozyme as a promising antioxidant to be loaded into cigarette filters. Moreover, biochar prepared through biomass pyrolysis endowed it with high thermal stability. Cellular and animal models showed that the biochar nanozyme loaded cigarette filter effectively protected lung tissues from vapor-phase free radicals in cigarette smoke.

## 2. EXPERIMENTAL SECTION

**2.1. Chemicals and Reagents.** Potassium permanganate ($KMnO_4$), sulfuric acid ($H_2SO_4$), nitric acid ($HNO_3$), phosphoric acid ($H_3PO_4$), sodium hydroxide (NaOH), sulfanilic acid, 1-naphthylamine, sodium nitrite ($NaNO_2$), and hydrogen peroxidase ($H_2O_2$, 30%) were purchased from Sinopharm Chemical Reagent Co., Ltd. (Shanghai, China). Nitro blue tetrazolium (NBT) and riboflavin were purchased from Sigma-Aldrich (St. Louis, USA). 4,5-Diaminofluorescein diacetate (DAF) was obtained from Adipogen Life Sciences (San Diego, USA). Glutathione (GSH) was obtained from Aladdin (Shanghai, China). All chemical reagents were used as received without further purification. All aqueous solutions used in the experiments were prepared with deionized water (18.2 MΩ·cm, Millipore).

**2.2. Instrumentation.** SEM images were obtained from an Ultra 55 (Zeiss, Germany) field emission scanning electron microscope (FE-SEM). TEM images were recorded on a JEM-2100 (JEOL, Japan) transmission electron microscope at an acceleration voltage of 200 kV. All the XRD data were recorded with 2 °/min on a diffractometer (Rigaku Ultima III, Japan) using Cu K$\alpha$ radiation. XPS spectra were collected by a PHI 5000 Versa Probe XPS microscope (Ulvac-Phi, Japan). Thermogravimetric analysis (TGA) was performed on an STA 449 F3 Jupiter apparatus (Netzsch, Germany) with a heating rate of 10 °C/min. Raman spectra were recorded using an inVia (Renishaw, Britain) Raman spectrometer. FT-IR spectra were recorded on a NEXUS-870 IR-spectrometer (Nicolet, USA). Fluorescence spectra were obtained on a Hitachi F-4600 spectrometer (Hitachi, Japan). $^1$H NMR spectra were obtained on a Bruker AM400 spectrometer (Bruker, Germany), and UV−vis spectra were obtained on a Cary UV−vis 100 spectrometer (Agilent, USA). Absorbance was recorded on a SpectraMax M2e microplate reader (Molecular Device, USA). The cell images were recorded on a BX53 fluorescence microscope (Olympus, Japan).

**2.3. Collection of Silkworm Excrement (SE).** Fresh SE was collected from silkworms we raised. Because the SE was usually mixed with leaf residues, we removed leaf residues and other impurities. After drying in a 60 °C oven, raw SE was obtained.

**2.4. Preparation of Calcined SE.** Typically, 100 mg of raw SE was placed in a crucible. Then, this covered crucible was placed in the center of a tube furnace and calcined at 600, 700, 800, and 900 °C for 2 h respectively under argon flow with a heating rate of 10 °C/min. After cooling, the calcined SE was obtained.

**2.5. SOD-like Activity of Calcined SE.** The $O_2^{\bullet-}$ was generated by irradiating riboflavin. For the comparison of SE calcined at different temperatures, riboflavin (1.2 mM), EDTA (0.1 M), 80 $\mu$L of different calcined SE samples (1 mg/mL), and NBT (0.1 mg/mL) were mixed in PBS buffer (10 mM, pH 7.4). The mixed solutions were then irradiated by a LED lamp (27 W) for 5 min.[42] The absorbance at 560 nm of the mixed solutions was then recorded by using a microplate reader. For the dose-dependent study, 20, 50, 80, 100, and 160 $\mu$L of SE900 was applied.

**2.6. Catalase-like Activity of Calcined SE.** For the comparison of SE calcined at different temperatures, 20 $\mu$L of different calcined SE samples (1 mg/mL) and $H_2O_2$ were added to PBS buffer (10 mM, pH 7.4) together. The final concentration of $H_2O_2$ applied in this work was 2 mM. After coincubation for 3 h at 37 °C, $H_2SO_4$ (4.5 M) and $KMnO_4$ (3.2 mM) were add to the above mixture; then, the absorbance at 525 nm was measured on a microplate reader. For the dose-dependent study, 5, 10, 20, 50, and 100 $\mu$L of SE900 was applied, and the reaction time was 30 min.

**2.7. Nitric Oxide Free Radical Scavenging Activity of Calcined SE.** GSNO was synthesized as described.[43] For the comparison of SE calcined at different temperatures, 50 $\mu$L of different calcined SE samples (1 mg/mL) and 100 $\mu$L of GSNO (0.1 mM) were added to PBS buffer (10 mM, pH 7.4); then, 1 $\mu$L of DAF (10 mM) was added into the mixture above immediately. After the reaction in the dark for 1 min, fluorescence spectra were measured under excitation at 495 nm. For the dose-dependent study, 20, 50, 100, and 150 $\mu$L of SE900 were applied.

**2.8. Free Radical Scavenging in Cigarette Smoke.** SE900 loaded cigarettes were prepared according to the method reported.[27] All the cigarettes in this work were Golden Dragon from Wuhan Tobacco Group. First, one-quarter of a cellulose acetate fiber was removed, and 50 mg of SE900 without grinding was placed into the original place. The $H_2O_2$ scavenging experiments were tested by the method mentioned above, and the absorbance of acid $KMnO_4$ (3.2 mM) was used for evaluating the $H_2O_2$ scavenging activity. NBT (0.1 mg/mL) in PBS buffer (10 mM, pH 7.4) was used for determining the levels of $O_2^{\bullet-}$. Saltzman reagent,[44] containing phosphoric acid ($H_3PO_4$), sulfanilic acid, and 1-naphthylamine, was used to detect $NO^{\bullet}$ specifically.

**2.9. Cytotoxicity Assay.** The mouse lung epithelial cell line was a gift from the Medical School of Nanjing University. The cells were cultured in Dulbecco's modified Eagle's medium (DMEM) supplemented with 10% fetal bovine serum (FBS), 0.1 mg/mL of streptomycin, and 100 U/mL of penicillin at 37 °C in an incubator supplied with a humidified atmosphere of 5% $CO_2$. CSE of each group was obtained by the setup in Figure 3a. Different concentrations of CSE (0.2, 2, and 20%) were used to coincubate with the mouse lung epithelial cell line for 2 h. After the coincubation, a CCK-8 assay was carried out to evaluate the cell viability. For live/dead staining, the CSE concentration was 10%. Typically, 2 $\mu$M calcein-AM (green) and 4 $\mu$M PI (red) were added to each group and incubated in the dark for 20 min. The stained cells were observed using a fluorescence microscope.

**2.10. *In Vivo* Smoking Model and H&E Staining.** All animal studies were performed under a protocol approved by the Animal Ethics Committee of Nanjing Drum Tower Hospital. ICR male mice (6−8 weeks old) were used in the smoking model. With the smoking system in Figure S9 (in the SI), after being placed into the container, mice were exposed to three cigarettes one time on three successive days. The flow rate was controlled at 0.2 L/min. In a control study, the normal mice were kept in a smoke-free environment. After the sacrifice of all the mice, the lung tissues were fixed with 4% paraformaldehyde and embedded in paraffin for H&E staining. The stained lung tissues were observed with optical microscopy.

**2.11. Cytokine Determination with an ELISA Kit Assay.** The lung tissues from each group were frozen and stored at −80 °C until the assays. Lung homogenates were prepared according to the protocols of different assays. The expression levels of TNF-$\alpha$, IL-1$\beta$, IL-10, and TGF-$\beta$1 were measured with a corresponding commercial


https://doi.org/10.1021/acsabm.1c01080
ACS Appl. Bio Mater. 2022, 5, 1831−1838

ELISA kit (Neobioscience, China) according to the manufacturer's protocols, respectively.

## 3. RESULTS AND DISCUSSION

**3.1. Calcined SE Preparation and Characterization.** As shown in Scheme 1, fresh SE was collected from silkworms we raised. In a typical process, the raw SE was obtained after removing the leaf residue and drying. The raw SE was then calcined in argon atmosphere at different temperatures (i.e., 600, 700, 800, and 900 °C) to prepare the biochar nanozymes. The calcined SE was denoted as SE600, SE700, SE800, and SE900. The four calcination temperatures were selected according to the quantitative thermogravimetric analysis (TGA) (Figure S1, in Supporting Information (SI)). At the temperatures higher than 900 °C, the mass loss was too great.

**Scheme 1. Biochar Nanozyme Derived from Silkworm Excrement for Scavenging Free Radicals of Cigarette Smoke**

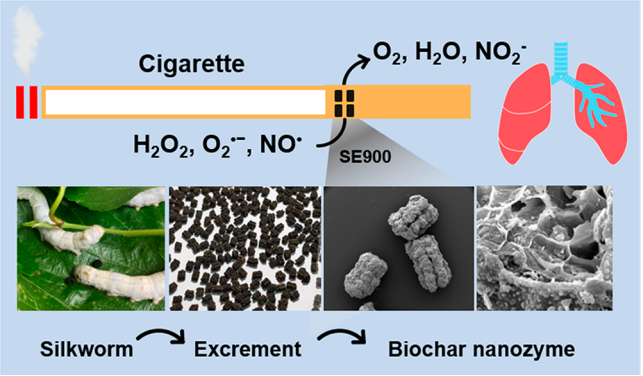


The morphology of the obtained biochar was investigated by scanning electron microscope (SEM) and transmission electron microscope (TEM). As shown in Figure 1a, the unique hierarchical porous structure of the raw SE (Figure S2, in the SI) was retained in SE900. The retained morphology during the calcination process could be attributed to the $CaCO_3$ and $SiO_2$ in raw SE, which would maintain the three-dimensional (3D) structure. It is worth noting that SE900 consisted of a very thin nanosheet structure confirmed by TEM (Figure 1b), which was formed by the raw SE biomass carbonization. The morphology of other calcined SE showed very similar results as that of SE900 (Figures S3 and S4, in the SI).

The 3D structure was further studied by the Brunauer–Emmett–Teller (BET) method, and the comparison of $N_2$ adsorption/desorption isotherm curves and the specific surface area ($S_{BET}$) results are displayed in Figure 1c. The $S_{BET}$ of these samples was 13.32, 35.74, 231.89, and 266.05 $m^2/g$, respectively. As the calcination temperature increases, the $S_{BET}$ of SE also increases. The higher $S_{BET}$ of SE900 endowed more active sites, which would benefit the free radical scavenging in cigarette smoke.

In the X-ray diffraction (XRD) pattern (Figure 1d), the characteristic peaks of calcite ($CaCO_3$) at $2\theta$ = 23.05, 29.40, 39.41, 56.56° and others were observed in all four samples. In SE900, the characteristic peak of calcium oxide (CaO) appeared because of the $CaCO_3$ decomposition. The $CaCO_3$ in SE900 played an important role in maintaining the structure. To confirm the existence of biochar in calcined SE, we etched the calcined SE using $HNO_3$ and NaOH. The four calcined SE samples after etching were characterized by XRD (Figure S5, in the SI) again, and the diffraction peaks around 26 and 42° confirmed the presence of the biochar.[45,46]

To investigate the chemical configuration of carbon elements, Raman spectra, X-ray photoelectron spectroscopy (XPS) spectra, and Fourier transform infrared spectroscopy (FT-IR) spectra were collected. It is known that the intensity ratio of peaks around 1360 and 1580 $cm^{-1}$ (ID/IG) is correlated with the disorder degree of carbon materials.[46] In Figure 1e, the calculated ID/IG ratios of the four calcined SE samples were 1.48, 1.33, 0.98, and 1.42, respectively. The disorder degree of the calcined SE decreased before the $CaCO_3$ decomposition at 900 °C. In the carbonization process of raw SE, the carbonization degree gradually increased, with the defects gradually decreasing. When the $CaCO_3$ was decomposed, the 3D structure would start to collapse, and the ID/IG value (disorder degree) increased to 1.42. In Figure S6 (in the SI), the XPS survey spectra of the samples showed

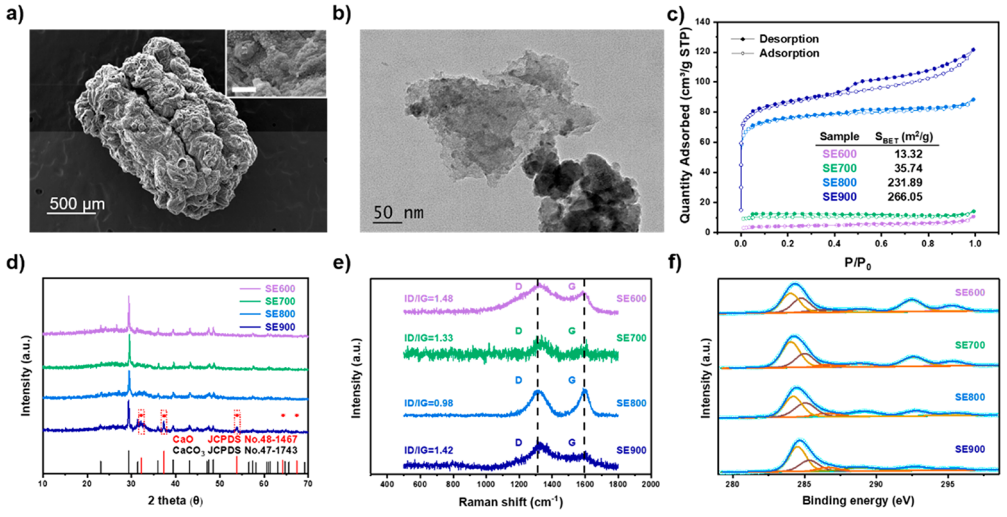


**Figure 1.** Structural characterization of the raw and calcined silkworm excrement (SE). (a) SEM and (b) TEM images of SE calcined at 900 °C (SE900). (Inset of a: magnified images; scale bar: 5 μm). (c) $N_2$ adsorption–desorption isotherm curves, (d) PXRD patterns, (e) Raman spectra, and (f) C 1s XPS spectra of SE calcined at different temperatures (600, 700, 800, and 900 °C).



https://doi.org/10.1021/acsabm.1c01080
ACS Appl. Bio Mater. 2022, 5, 1831–1838

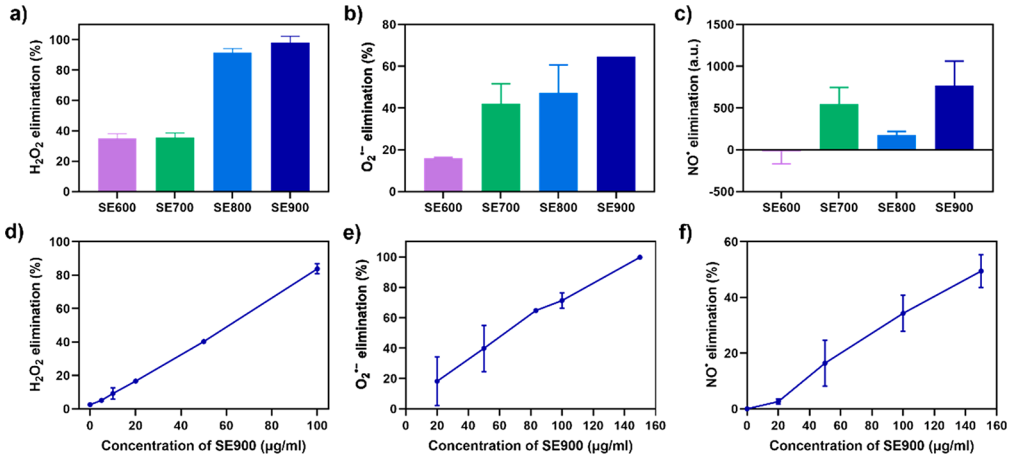


**Figure 2.** Free radical scavenging properties of calcined SE. (a,d) $H_2O_2$ scavenging catalyzed by the catalase-like activity of indicated materials. (b,e) $O_2^{\bullet-}$ elimination catalyzed by the SOD-like activity of indicated materials. (c,f) NO• elimination catalyzed by NO• scavenging activity of indicated materials. Data are presented as mean ± standard error of the mean ($n$ = 3).

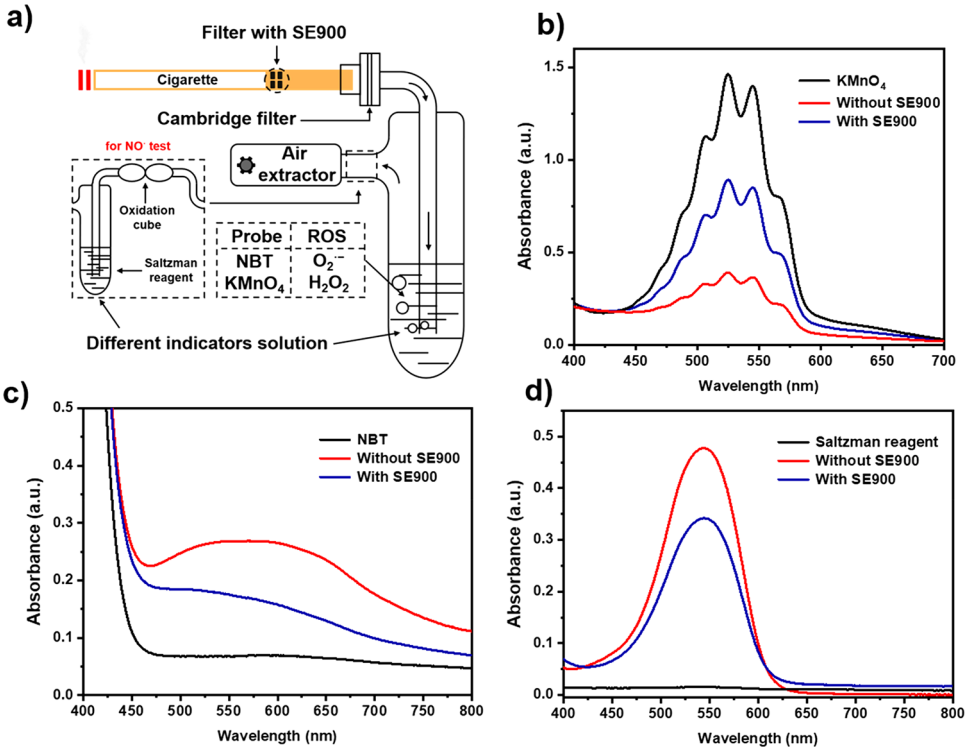


**Figure 3.** Effective free radical scavenging in cigarette smoke by an SE900 loaded cigarette filter. (a) Schematic of the setup to test the level of free radicals in cigarette smoke extract. (b) Absorption spectra of $KMnO_4$, the $H_2O_2$ indicator, under indicated conditions. (c) Absorption spectra of NBT, the $O_2^{\bullet-}$ probe, under indicated conditions. (d) Absorption spectra of Saltzman reagent, the NO• probe, under indicated conditions.

obvious peaks of C 1s, Ca 2p, and O 1s, consistent with the results obtained by XRD. The high-resolution C 1s XPS spectra (Figure 1f) showed that the carbon element consisted of six main fitting components, C−C, C=C, C−O, C−O−Ca, $C-CO_3$, and −COOH moieties. The binding energy of C−C/C=C and C−O (Table S1, in the SI) increased with the elevation of temperature, which accounts for the increasing carbonization degree. In the FT-IR spectra (Figure S7, in the SI), the similar C−O and O−H stretching vibration and bending vibration were observed in all four samples.

**3.2. Free Radical Scavenging Properties of Calcined SE.** To investigate the free radical scavenging properties of calcined SE, we selected two representative ROS ($H_2O_2$ and $O_2^{\bullet-}$) and one representative RNS (NO•).[47] Correspondingly, we investigated the enzyme-like activities, including the catalase-like activity, SOD-like activity, and NO• scavenging activity. In the SOD-like activity assay, nitro blue tetrazolium (NBT) was used to evaluate $O_2^{\bullet-}$ (generated from the irradiation of riboflavin) scavenging activity.[42] Because the violet $KMnO_4$ in acid conditions would be reduced to colorless species by $H_2O_2$, we used this method to evaluate the catalase-like activity of calcined SE.[48] To assess the NO• scavenging capability of calcined SE, *S*-nitroso-glutathione (GSNO), a precursor which could release NO• gradually, was used to generate NO•.[49] The synthesis of GSNO was confirmed by 400 MHz $^1$H nuclear magnetic resonance (NMR) spectra


https://doi.org/10.1021/acsabm.1c01080
ACS Appl. Bio Mater. 2022, 5, 1831−1838

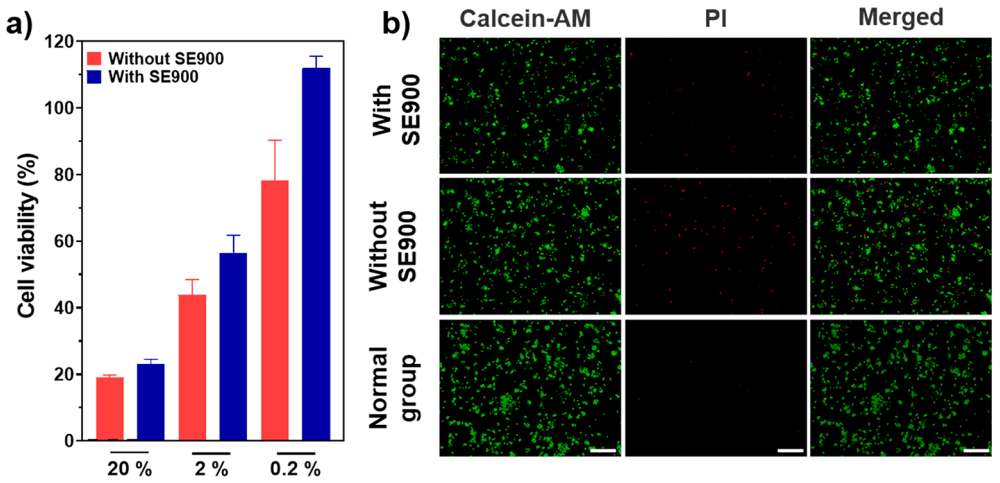


**Figure 4.** Scavenging free radicals of cigarette smoke for cell protection. (a) Cytotoxicity of cigarette smoke extract (CSE) produced with a normal cigarette and a cigarette loaded with SE900 (20, 2, 0.2%: concentrations of CSE). Data are presented as mean ± standard error of the mean ($n$ = 5). (b) Dead−live staining of a mouse lung epithelial cell line treated with CSE (10%) produced with a normal cigarette and a cigarette loaded with SE900 as well as a normally cultured cell line (without a cigarette). (Scale bars: 200 $\mu$m.)

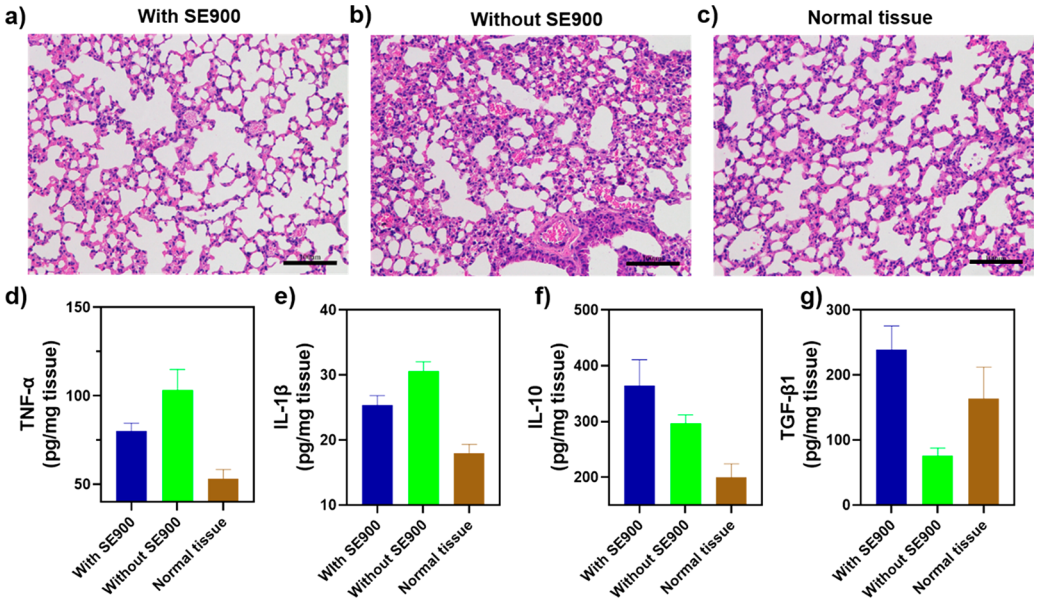


**Figure 5.** Scavenging free radicals of cigarette smoke to minimize the cigarette-smoke-induced lung injury in a mouse model. H&E staining of lung tissues of mice treated with (a) an SE900 loaded cigarette and (b) without SE900 (normal cigarette) as well as (c) normal mice (without cigarette smoke). (Scale bar: 100 $\mu$m.) Levels of (d) TNF-$\alpha$, (e) IL-1$\beta$, (f) IL-10, and (g) TFG-$\beta$1 in the lung tissues of mice under different treatments. Data are presented as mean ± standard error of the mean ($n$ = 5).

(Figure S8, in the SI).[43] The fluorescence intensity changes of 4,5-diaminofluorescein diacetate (DAF, a probe that could specifically detect $NO^{\bullet}$) were used to evaluate the $NO^{\bullet}$ scavenging activity.[50] As shown in Figure 2a−c, SE900 exhibited the highest free radical scavenging activities over the other SE samples, both for ROS and RNS. We inferred the highest activities of SE900 may originate from the higher carbonization and disorder degree, confirmed by the XPS (higher binding energy of C−C/C=C) and Raman results, caused by higher temperature. Moreover, the higher surface area of SE900 supports more active sites to scavenge free radicals. As shown in Figure 2d−f, the curves showed a positive correlation between the three kinds of radical scavenging activities and the concentrations of SE900.

**3.3. Free Radical Scavenging in Cigarette Smoke by an SE900 Nanozyme Loaded Filter.** To investigate the free scavenging efficiency in cigarette smoke, we prepared cigarettes with SE900 nanozyme loaded filters. We then collected the cigarette smoke extract (CSE).[51] As shown in Figure 3a, the homemade setup was used to simulate the process of smoking. The tar, nicotine, and particulate matter that would interfere with the detection of indicators were adsorbed by the Cambridge filter shown in Figure 3a.[52] After passing through the Cambridge filter, the vapor-phase free radicals in a cigarette would dissolve into the buffer solution containing free radical indicators. The acid $KMnO_4$ and NBT were placed into the tube which contained the CSE inhaled by an air extractor to evaluate the levels of $H_2O_2$ and $O_2^{\bullet-}$. To exclude the interference of another RNS, the nitrogen dioxide radical


https://doi.org/10.1021/acsabm.1c01080
ACS Appl. Bio Mater. 2022, 5, 1831−1838

($NO_2^{\bullet}$), the $CrO_3$ oxidation tube, and another tube containing Saltzman reagent were added between the original tube and the air extractor. The knob on an air extractor could adjust the flow rate of cigarette smoke to control the same concentration of CSE in each group. As shown in Figure 3b–d, three kinds of free radicals (*i.e.*, $H_2O_2$, $O_2^{\bullet-}$, and $NO^{\bullet}$) in cigarette smoke were scavenged effectively by the SE900 biochar nanozyme loaded in filter.

**3.4. SE900 Nanozyme Protected Cells from Cigarette Smoke *in Vitro*.** To investigate the effects of SE900 on free radicals in cigarette-smoke-induced cell death *in vitro*, a mouse lung epithelial cell line was cultured with CSE. The CSE of the cigarette whose filter was loaded with SE900 and the conventional one was collected with the same method mentioned above. Using the Cell Counting Kit-8 (CCK-8) assay, it was found that the SE900 group had better cell viability than the conventional cigarette group at all the CSE concentrations (20, 10, and 2%) (Figure 4a).

To confirm the above results, we performed live/dead staining to observe cells treated with different CSE concentrations and normal cells. The cells were stained by calcein-AM and propidium iodide (PI) double-staining to distinguish live and dead cells (Figure 4b). In the SE900 loaded cigarette group, the ratio of dead cells was lower than that of the conventional cigarette group, which showed that the SE900 loaded cigarette filter could protect lung tissue from free radicals in cigarette smoke.

**3.5. SE900 Nanozyme Protected Lung Tissue from Cigarette Smoke *in Vivo*.** Based on the excellent antioxidant properties and the cellular experiments results *in vitro*, we advanced to an *in vivo* passive smoking model to investigate the effect of the cigarette loaded with SE900. As shown in Figure S9 (in the SI), a smoking system was constructed by a sealed container equipped with a homemade air extractor.[27] After mice were placed into the smoking system, cigarette smoke passed through the filter with or without SE900 being channeled into the container. Mice were sacrificed after the consecutive exposure to cigarette smoke for 3 days, and the entire lungs were collected for the following hematoxylin and eosin (H&E) staining and enzyme linked immunosorbent assay (ELISA) analysis. As shown in Figure 5a–c, compared with the group without SE900, the group with the SE900 loaded filter showed decreased inflammatory cell infiltration to a normal thickness of bronchi capillary walls and a nearly normal histological microstructure. These results indicated the SE900 nanozyme could effectively alleviate lung tissue damage by scavenging the free radicals in cigarette smoke. Furthermore, the expression levels of tumor necrosis factor (TNF)-$\alpha$, interleukin (IL)-1$\beta$, IL-10, and transforming growth factor (TGF)-$\beta$1 in lung tissue were evaluated by ELISA. As shown in Figure 5d,e, the decreased levels of proinflammatory cytokines TNF-$\alpha$ and IL-1$\beta$ and the increased level of anti-inflammatory cytokine IL-10 (Figure 5f) in the SE900 loaded group indicated that SE900 could protect lung tissues from oxidative stress by regulating the levels of inflammatory cytokines.[53−55] Additionally, the levels of TGF-$\beta$1 (Figure 5g) were also upregulated because of the SE900 loaded in the filter, suggesting a better tissue repair potential of mice in the SE900 loaded group.[56] The above results demonstrated that SE900 could alleviate oxidative stress by scavenging free radicals and regulating the levels of inflammatory-related cytokines in the lungs of mice exposed to cigarette smoke. The comparison with previous nanozymes used in cigarette filter is listed in Table S2.

## 4. CONCLUSIONS

In conclusion, we demonstrated a biochar nanozyme derived from silkworm excrement. The biochar nanozyme has been proved to possess antioxidant properties of scavenging excess free radicals including ROS and RNS. Further, both the *in vitro* and *in vivo* experiments demonstrated the obtained biochar nanozyme loaded in a cigarette filter could effectively protect the lung tissue of mice exposed to cigarette smoke. This work not only demonstrated a potent biochar nanozyme to protect lung tissue from cigarette smoke but also provided new scenes to rationally utilize biowaste resources.

## ■ ASSOCIATED CONTENT

### Supporting Information

The Supporting Information is available free of charge at https://pubs.acs.org/doi/10.1021/acsabm.1c01080.

Binding energy of C 1s in XPS analysis (Table S1), comparison of nanozymes used in a cigarette filter (Table S2), thermogravimetric analysis (TGA) of raw SE under $N_2$ (Figure S1), SEM image of raw SE (Figure S2), SEM images of SE600, SE700, and SE800 (Figure S3), TEM images of SE600, SE700, and SE800 (Figure S4), XRD patterns of the calcined SE etched by $HNO_3$ and NaOH (Figure S5), XPS survey spectra of the calcined SE (Figure S6), FT-IR spectra of the calcined SE (Figure S7), $^1H$ NMR spectrum of GSNO (Figure S8), and the schematic of the setup for the animal study (Figure S9) (PDF)

## ■ AUTHOR INFORMATION


### Corresponding Authors

**Yan Du** − *State Key Laboratory of Electroanalytical Chemistry, Changchun Institute of Applied Chemistry, Chinese Academy of Sciences, Changchun, Jilin 130022, China; University of Science and Technology of China, Hefei, Anhui 230026, China;* orcid.org/0000-0003-3197-7204; Email: duyan@ciac.ac.cn, duyan.bessie@gmail.com

**Hui Wei** − *Department of Biomedical Engineering, College of Engineering and Applied Sciences, Nanjing National Laboratory of Microstructures, Jiangsu Key Laboratory of Artificial Functional Materials, Nanjing University, Nanjing, Jiangsu 210023, China; State Key Laboratory of Analytical Chemistry for Life Science, School of Chemistry and Chemical Engineering, Chemistry and Biomedicine Innovation Center (ChemBIC), Nanjing University, Nanjing, Jiangsu 210023, China;* orcid.org/0000-0003-0870-7142; Email: weihui@nju.edu.cn

### Authors

**Quanyi Liu** − *State Key Laboratory of Electroanalytical Chemistry, Changchun Institute of Applied Chemistry, Chinese Academy of Sciences, Changchun, Jilin 130022, China; University of Science and Technology of China, Hefei, Anhui 230026, China*

**Sheng Zhao** − *Department of Biomedical Engineering, College of Engineering and Applied Sciences, Nanjing National Laboratory of Microstructures, Jiangsu Key Laboratory of Artificial Functional Materials, Nanjing University, Nanjing, Jiangsu 210023, China*




https://doi.org/10.1021/acsabm.1c01080
ACS Appl. Bio Mater. 2022, 5, 1831−1838

**Yihong Zhang** − *Department of Biomedical Engineering, College of Engineering and Applied Sciences, Nanjing National Laboratory of Microstructures, Jiangsu Key Laboratory of Artificial Functional Materials, Nanjing University, Nanjing, Jiangsu 210023, China*

**Xueying An** − *State Key Laboratory of Pharmaceutical Biotechnology and Jiangsu Key Laboratory of Molecular Medicine, Nanjing University Medical School, Nanjing, Jiangsu 210023, China; Department of Sports Medicine and Adult Reconstructive Surgery, Nanjing Drum Tower Hospital, The Affiliated Hospital of Nanjing University Medical School, Nanjing, Jiangsu 210093, China*

**Quan Wang** − *Department of Biomedical Engineering, College of Engineering and Applied Sciences, Nanjing National Laboratory of Microstructures, Jiangsu Key Laboratory of Artificial Functional Materials, Nanjing University, Nanjing, Jiangsu 210023, China*

**Sirong Li** − *Department of Biomedical Engineering, College of Engineering and Applied Sciences, Nanjing National Laboratory of Microstructures, Jiangsu Key Laboratory of Artificial Functional Materials, Nanjing University, Nanjing, Jiangsu 210023, China*

**Anqi Lin** − *Department of Biomedical Engineering, College of Engineering and Applied Sciences, Nanjing National Laboratory of Microstructures, Jiangsu Key Laboratory of Artificial Functional Materials, Nanjing University, Nanjing, Jiangsu 210023, China*

Complete contact information is available at: https://pubs.acs.org/10.1021/acsabm.1c01080

### Notes

The authors declare no competing financial interest.

## ■ ACKNOWLEDGMENTS

This work was supported by the National Natural Science Foundation of China (21874067 and 21874129), the National Key R&D Program of China (2019YFA0709200), CAS Interdisciplinary Innovation Team (JCTD-2020-08), PAPD Program, Fundamental Research Funds for the Central Universities (021314380195), and the International Scientific Cooperation Project of Jilin Scientific and Technological Development Program (20200801044GH).

## ■ REFERENCES

(1) Carnevali, S.; Petruzzelli, S.; Longoni, B.; Vanacore, R.; Barale, R.; Cipollini, M.; Scatena, F.; Paggiaro, P.; Celi, A.; Giuntini, C. Cigarette smoke extract induces oxidative stress and apoptosis in human lung fibroblasts. *Am. J. Physiol.: Lung Cell. Mol. Physiol.* **2003**, *284*, L955−963.

(2) Csordas, A.; Bernhard, D. The biology behind the atherothrombotic effects of cigarette smoke. *Nat. Rev. Cardiol.* **2013**, *10*, 219−230.

(3) Staempfli, M. R.; Anderson, G. P. How cigarette smoke skews immune responses to promote infection, lung disease and cancer. *Nat. Rev. Immunol.* **2009**, *9*, 377−384.

(4) *WHO report on the global tobacco epidemic 2019: Offer help to quit tobacco use*; World Health Organization, 2019.

(5) BLUHM, A. L.; WEINSTEIN, J.; SOUSA, J. A. Free Radicals in Tobacco Smoke. *Nature* **1971**, *229*, 500.

(6) Norman, V.; Keith, C. H. Nitrogen Oxides in Tobacco Smoke. *Nature* **1965**, *205*, 915−916.

(7) PRYOR, W. A.; STONE, K. Oxidants in Cigarette Smoke Radicals, Hydrogen Peroxide, Peroxynitrate, and Peroxynitrite. *Ann. N. Y. Acad. Sci.* **1993**, *686*, 12−27.

(8) Onizawa, S.; Aoshiba, K.; Kajita, M.; Miyamoto, Y.; Nagai, A. Platinum nanoparticle antioxidants inhibit pulmonary inflammation in mice exposed to cigarette smoke Pulm. *Pulm. Pharmacol. Ther.* **2009**, *22*, 340−349.

(9) Liu, L. Z.; Yu, W.; Luo, D.; Xue, Z. J.; Qin, X. Y.; Sun, X. H.; Zhao, J. C.; Wang, J. L.; Wang, T. Catalase Nanocapsules Protected by Polymer Shells for Scavenging Free Radicals of Tobacco Smoke. *Adv. Funct. Mater.* **2015**, *25*, 5159−5165.

(10) Wei, H.; Wang, E. Nanomaterials with enzyme-like characteristics (nanozymes): next-generation artificial enzymes. *Chem. Soc. Rev.* **2013**, *42*, 6060−6093.

(11) Wu, J.; Wang, X.; Wang, Q.; Lou, Z.; Li, S.; Zhu, Y.; Qin, L.; Wei, H. Nanomaterials with enzyme-like characteristics (nanozymes): next-generation artificial enzymes (II). *Chem. Soc. Rev.* **2019**, *48*, 1004−1076.

(12) Huang, Y.; Ren, J.; Qu, X. Nanozymes: classification, catalytic mechanisms, activity regulation, and applications. *Chem. Rev.* **2019**, *119*, 4357−4412.

(13) Jiang, D.; Ni, D.; Rosenkrans, Z. T.; Huang, P.; Yan, X.; Cai, W. Nanozyme: new horizons for responsive biomedical applications. *Chem. Soc. Rev.* **2019**, *48*, 3683−3704.

(14) Kang, T.; Kim, Y. G.; Kim, D.; Hyeon, T. Inorganic nanoparticles with enzyme-mimetic activities for biomedical applications. *Coord. Chem. Rev.* **2020**, *403*, 213092.

(15) Tang, G.; He, J.; Liu, J.; Yan, X.; Fan, K. Nanozyme for tumor therapy: Surface modification matters. *Exploration* **2021**, *1*, 75−89.

(16) Zhang, R.; Yan, X.; Fan, K. Nanozymes Inspired by Natural Enzymes. *Acc. Mater. Res.* **2021**, *2*, 534−547.

(17) Wei, H.; Gao, L.; Fan, K.; Liu, J.; He, J.; Qu, X.; Dong, S.; Wang, E.; Yan, X. Nanozymes: A clear definition with fuzzy edges. *Nano Today* **2021**, *40*, 101269.

(18) Gao, L.; Zhuang, J.; Nie, L.; Zhang, J.; Zhang, Y.; Gu, N.; Wang, T.; Feng, J.; Yang, D.; Perrett, S.; Yan, X. Intrinsic peroxidase-like activity of ferromagnetic nanoparticles. *Nat. Nanotechnol.* **2007**, *2*, 577−583.

(19) Huang, L.; Chen, J.; Gan, L.; Wang, J.; Dong, S. Single-atom nanozymes. *Sci. Adv.* **2019**, *5*, No. eaav5490.

(20) Shen, X.; Liu, W.; Gao, X.; Lu, Z.; Wu, X.; Gao, X. Mechanisms of oxidase and superoxide dismutation-like activities of gold, silver, platinum, and palladium, and their alloys: a general way to the activation of molecular oxygen. *J. Am. Chem. Soc.* **2015**, *137*, 15882−15891.

(21) Xu, C.; Qu, X. Cerium oxide nanoparticle: a remarkably versatile rare earth nanomaterial for biological applications. *NPG Asia Mater.* **2014**, *6*, No. e90.

(22) Tonga, G. Y.; Jeong, Y.; Duncan, B.; Mizuhara, T.; Mout, R.; Das, R.; Kim, S. T.; Yeh, Y.-C.; Yan, B.; Hou, S.; Rotello, V. M. Supramolecular regulation of bioorthogonal catalysis in cells using nanoparticle-embedded transition metal catalysts. *Nat. Chem.* **2015**, *7*, 597.

(23) Zhang, Z.; Zhang, X.; Liu, B.; Liu, J. Molecular imprinting on inorganic nanozymes for hundred-fold enzyme specificity. *J. Am. Chem. Soc.* **2017**, *139*, 5412−5419.

(24) Zhang, W.; Hu, S.; Yin, J. J.; He, W.; Lu, W.; Ma, M.; Gu, N.; Zhang, Y. Prussian blue nanoparticles as multienzyme mimetics and reactive oxygen species scavengers. *J. Am. Chem. Soc.* **2016**, *138*, 5860−5865.

(25) Soh, M.; Kang, D. W.; Jeong, H. G.; Kim, D.; Kim, D. Y.; Yang, W.; Song, C.; Baik, S.; Choi, I. Y.; Ki, S. K.; Kwon, H. J.; Kim, T.; Kim, C. K.; Lee, S. H.; Hyeon, T. Ceria-Zirconia nanoparticles as an enhanced multi-antioxidant for sepsis treatment. *Angew. Chem., Int. Ed.* **2017**, *56*, 11399−11403.

(26) Korschelt, K.; Ragg, R.; Metzger, C. S.; Kluenker, M.; Oster, M.; Barton, B.; Panthofer, M.; Strand, D.; Kolb, U.; Mondeshki, M.; Strand, S.; Brieger, J.; Nawaz Tahir, M.; Tremel, W. Glycine-functionalized copper(ii) hydroxide nanoparticles with high intrinsic superoxide dismutase activity. *Nanoscale* **2017**, *9*, 3952−3960.

(27) Lin, S.; Cheng, Y.; Zhang, H.; Wang, X.; Zhang, Y.; Zhang, Y.; Miao, L.; Zhao, X.; Wei, H. Copper tannic acid coordination

nanosheet: a potent nanozyme for scavenging ROS from cigarette smoke. *Small* **2020**, *16*, No. 1902123.
(28) Zhou, X.; Zeng, W.; Rong, S.; Lv, H.; Chen, Y.; Mao, Y.; Tan, W.; Li, H. Alendronate-Modified Nanoceria with Multiantioxidant Enzyme-Mimetic Activity for Reactive Oxygen Species/Reactive Nitrogen Species Scavenging from Cigarette Smoke. *ACS Appl. Mater. Interfaces* **2021**, *13*, 47394−47406.
(29) Sun, H.; Zhou, Y.; Ren, J.; Qu, X. Carbon Nanozymes: Enzymatic Properties, Catalytic Mechanism, and Applications. *Angew. Chem., Int. Ed.* **2018**, *57*, 9224−9237.
(30) Ding, H.; Hu, B.; Zhang, B.; Zhang, H.; Yan, X. Y.; Nie, G. H.; Liang, M. M. Carbon-based nanozymes for biomedical applications. *Nano Res.* **2021**, *14*, 570−583.
(31) Samuel, E. L.; Marcano, D. C.; Berka, V.; Bitner, B. R.; Wu, G.; Potter, A.; Fabian, R. H.; Pautler, R. G.; Kent, T. A.; Tsai, A. L.; Tour, J. M. Highly efficient conversion of superoxide to oxygen using hydrophilic carbon clusters. *Proc. Natl. Acad. Sci. U. S. A.* **2015**, *112*, 2343−2348.
(32) Fan, K.; Xi, J.; Fan, L.; Wang, P.; Zhu, C.; Tang, Y.; Xu, X.; Liang, M.; Jiang, B.; Yan, X.; Gao, L. In vivo guiding nitrogen-doped carbon nanozyme for tumor catalytic therapy. *Nat. Commun.* **2018**, *9*, 1440.
(33) Mu, X.; He, H.; Wang, J.; Long, W.; Li, Q.; Liu, H.; Gao, Y.; Ouyang, L.; Ren, Q.; Sun, S.; Wang, J.; Yang, J.; Liu, Q.; Sun, Y.; Liu, C.; Zhang, X. D.; Hu, W. Carbogenic Nanozyme with Ultrahigh Reactive Nitrogen Species Selectivity for Traumatic. *Nano Lett.* **2019**, *19*, 4527−4534.
(34) Wang, L.; Li, B.; Li, L.; Xu, F.; Xu, Z.; Wei, D.; Feng, Y.; Wang, Y.; Jia, D.; Zhou, Y. Ultrahigh-yield synthesis of N-doped carbon nanodots that down-regulate ROS in zebrafish. *J. Mater. Chem. B* **2017**, *5*, 7848−7860.
(35) Rizzo, C.; Arcudi, F.; Dordevic, L.; Dintcheva, N. T.; Noto, R.; D'Anna, F.; Prato, M. Nitrogen-Doped Carbon Nanodots-Ionogels: Preparation, Characterization, and Radical Scavenging Activity. *ACS Nano* **2018**, *12*, 1296−1305.
(36) Li, F.; Li, T.; Sun, C.; Xia, J.; Jiao, Y.; Xu, H. Selenium-Doped Carbon Quantum Dots for Free-Radical Scavenging. *Angew. Chem., Int. Ed.* **2017**, *56*, 9910−9914.
(37) Chen, X.; Zhao, L.; Wu, K.; Yang, H.; Zhou, Q.; Xu, Y.; Zheng, Y.; Shen, Y.; Liu, S.; Zhang, Y. Bound oxygen-atom transfer endows peroxidase-mimic M-N-C with high substrate selectivity. *Chem. Sci.* **2021**, *12*, 8865−8871.
(38) Chen, X.; Zhu, C.; Xu, Y.; Wang, K.; Cao, X.; Shen, Y.; Liu, S.; Zhang, Y. Quantitative evaluation of $O_2$ activation half-reaction for Fe−N−C in oxidase-like activity enhancement. *Catal. Sci. Technol.* **2021**, *11*, 7255−7259.
(39) Qian, K.; Kumar, A.; Zhang, H.; Bellmer, D.; Huhnke, R. Recent advances in utilization of biochar Renewable Sustainable Energy. *Renewable Sustainable Energy Rev.* **2015**, *42*, 1055−1064.
(40) Zhang, R.; Rao, Z. G.; Li, Y.; Li, H. Y.; Fei, L. F.; Lei, S. J.; Wang, Y. Silkworm Excrement Derived In-situ Co-doped Nanoporous Carbon as Confining Sulfur Host for Lithium Sulfur Batteries. *Chemistryselect* **2019**, *4*, 5678−5685.
(41) Lei, S.; Chen, L.; Zhou, W.; Deng, P.; Liu, Y.; Fei, L.; Lu, W.; Xiao, Y.; Cheng, B. Tetra-heteroatom self-doped carbon nanosheets derived from silkworm excrement for high-performance supercapacitors. *J. Power Sources* **2018**, *379*, 74−83.
(42) Liu, Y.; Zhang, Y.; Liu, Q.; Wang, Q.; Lin, A.; Luo, J.; Du, Y.; Lin, Y. W.; Wei, H. In vitro measurement of superoxide dismutase-like nanozyme activity: a comparative study. *Analyst* **2021**, *146*, 1872−1879.
(43) Lutzke, A.; Melvin, A. C.; Neufeld, M. J.; Allison, C. L.; Reynolds, M. M. Nitric oxide generation from S-nitrosoglutathione: New activity of indium and a survey of metal ion effects. *Nitric Oxide* **2019**, *84*, 16−21.
(44) Tsikas, D. Analysis of nitrite and nitrate in biological fluids by assays based on the Griess reaction: appraisal of the Griess reaction in the L-arginine/nitric oxide area of research. *J. Chromatogr. B: Anal. Technol. Biomed. Life Sci.* **2007**, *851*, 51−70.
(45) Wang, P.; Zhang, G.; Li, M. Y.; Yin, Y. X.; Li, J. Y.; Li, G.; Wang, W. P.; Peng, W.; Cao, F. F.; Guo, Y. G. Porous carbon for high-energy density symmetrical supercapacitor and lithium-ion hybrid electrochemical capacitors. *Chem. Eng. J.* **2019**, *375*, 122020.
(46) Ferrari, A. C.; Basko, D. M. Raman spectroscopy as a versatile tool for studying the properties of graphene. *Nat. Nanotechnol.* **2013**, *8*, 235−246.
(47) Chen, T.; Zou, H.; Wu, X.; Liu, C.; Situ, B.; Zheng, L.; Yang, G. Nanozymatic Antioxidant System Based on $MoS_2$ Nanosheets. *ACS Appl. Mater. Interfaces* **2018**, *10*, 12453−12462.
(48) Wang, Y. J.; Dong, H.; Lyu, G. M.; Zhang, H. Y.; Ke, J.; Kang, L. Q.; Teng, J. L.; Sun, L. D.; Si, R.; Zhang, J.; Liu, Y. J.; Zhang, Y. W.; Huang, Y. H.; Yan, C. H. Engineering the defect state and reducibility of ceria based nanoparticles for improved anti-oxidation performance. *Nanoscale* **2015**, *7*, 13981−13990.
(49) Yang, T.; Fruergaard, A. S.; Winther, A. K.; Zelikin, A. N.; Chandrawati, R. Zinc Oxide Particles Catalytically Generate Nitric Oxide from Endogenous and Exogenous Prodrugs. *Small* **2020**, *16*, No. 1906744.
(50) Kojima, H.; Nakatsubo, N.; Kikuchi, K.; Kawahara, S.; Kirino, Y.; Nagoshi, H.; Hirata, Y.; Nagano, T. Detection and imaging of nitric oxide with novel fluorescent indicators: diaminofluoresceins. *Anal. Chem.* **1998**, *70*, 2446−2453.
(51) Hoshino, Y.; Mio, T.; Nagai, S.; Miki, H.; Ito, I.; Izumi, T. Cytotoxic effects of cigarette smoke extract on an alveolar type II cell-derived cell line. *Am. J. Physiol.: Lung Cell. Mol. Physiol.* **2001**, *281*, L509−516.
(52) Lu, X.; Hua, Z.; Du, G.; Ma, X.; Cao, J.; Yang, Z.; Chen, J. Scavenging of free radicals in gas-phase mainstream cigarette smoke by immobilized catalase at filter level Free. *Free Radical Res.* **2008**, *42*, 244−252.
(53) Zhao, S.; Li, Y. X.; Liu, Q. Y.; Li, S. R.; Cheng, Y.; Cheng, C. Q.; Sun, Z. Y.; Du, Y.; Butch, C. J.; Wei, H. An orally administered $CeO_2$@montmorillonite nanozyme targets inflammation for inflammatory bowel disease therapy. *Adv. Funct. Mater.* **2020**, *30*, 2004692.
(54) Sun, L.; Louie, M. C.; Vannella, K. M.; Wilke, C. A.; LeVine, A. M.; Moore, B. B.; Shanley, T. P. New concepts of IL-10-induced lung fibrosis: fibrocyte recruitment and M2 activation in a CCL2/CCR2 axis. *Am. J. Physiol.: Lung Cell. Mol. Physiol.* **2011**, *300*, L341−353.
(55) Bry, K.; Whitsett, J. A.; Lappalainen, U. IL-1beta disrupts postnatal lung morphogenesis in the mouse. *Am. J. Respir. Cell Mol. Biol.* **2007**, *36*, 32−42.
(56) Togo, S.; Holz, O.; Liu, X.; Sugiura, H.; Kamio, K.; Wang, X.; Kawasaki, S.; Ahn, Y.; Fredriksson, K.; Skold, C. M.; Mueller, K. C.; Branscheid, D.; Welker, L.; Watz, H.; Magnussen, H.; Rennard, S. I. Lung fibroblast repair functions in patients with chronic obstructive pulmonary disease are altered by multiple mechanisms. *Am. J. Respir. Crit. Care Med.* **2008**, *178*, 248−260.


https://doi.org/10.1021/acsabm.1c01080
*ACS Appl. Bio Mater.* 2022, 5, 1831−1838